The Transit Light Curve Project. X. A Christmas Transit of HD 17156b

Joshua N. Winn[1], Matthew J. Holman[2], Gregory W. Henry[3], Guillermo Torres[2], Debra Fischer[4], John Asher Johnson[5,6], Geoffrey W. Marcy[7], Avi Shporer[8], Tsevi Mazeh[8]

ABSTRACT

Photometry is presented of the Dec. 25, 2007 transit of HD 17156b, which has the longest orbital period and highest orbital eccentricity of all the known transiting exoplanets. New measurements of the stellar radial velocity are also presented. All the data are combined and integrated with stellar-evolutionary modeling to derive refined system parameters. The planet's mass and radius are found to be $3.212^{+0.069}_{-0.082}$ $M_{\rm Jup}$ and $1.023^{+0.070}_{-0.055}$ $R_{\rm Jup}$. The corresponding stellar properties are $1.263^{+0.035}_{-0.047}$ $M_\odot$ and $1.446^{+0.099}_{-0.067}$ $R_\odot$. The planet is smaller by 1σ than a theoretical solar-composition gas giant with the same mass and equilibrium temperature, a possible indication of heavy-element enrichment. The midtransit time is measured to within 1 min, and shows no deviation from a linear ephemeris (and therefore no evidence for orbital perturbations from other planets). We provide ephemerides for future transits and superior conjunctions. There is an 18% chance that the orbital plane is oriented close enough to edge-on for secondary eclipses to occur at superior conjunction. Observations of secondary eclipses would reveal the thermal emission spectrum of a planet that experiences unusually large tidal heating and insolation variations.

Subject headings: planetary systems — stars: individual (HD 17156)

[1]Department of Physics, and Kavli Institute for Astrophysics and Space Research, Massachusetts Institute of Technology, Cambridge, MA 02139, USA

[2]Harvard-Smithsonian Center for Astrophysics, 60 Garden Street, Cambridge, MA 02138, USA

[3]Center of Excellence in Information Systems, Tennessee State University, 3500 John A. Merritt Blvd., Box 9501, Nashville, TN 37209, USA

[4]Department of Physics and Astronomy, San Francisco State University, San Francisco, CA 94132

[5]Institute for Astronomy, University of Hawaii, Honolulu, HI 96822

[6]NSF Astronomy & Astrophysics Postdoctoral Fellow

[7]Department of Astronomy, University of California, Mail Code 3411, Berkeley, CA 94720

[8]Wise Observatory, Tel Aviv University, Tel Aviv, Israel 69978

1. Introduction

It is possible to estimate the mass and radius of a transiting planet using a combination of photometry, Doppler data, and stellar modeling, just as has long been done for eclipsing binary stars (Vogel 1890). Some aspects of the planetary orbit and atmosphere can also be measured through high-precision transit photometry and spectroscopy (see, e.g., Charbonneau et al. 2007, Seager 2008, Winn 2008). These opportunities are more likely to occur for short-period planets, because the probability for a randomly-oriented orbit to be viewed close enough to edge-on for transits declines as $P^{-2/3}$. This explains why all but one of the known transiting planets have periods smaller than 10 days.

The exception is HD 17156b, for which $P = 21.2$ days. This planet was discovered in a Doppler survey by Fischer et al. (2007). The probability for transits to occur was larger than one might have guessed based only on the period, because the planet is near pericenter at the time of inferior conjunction (see, e.g., Burke 2008, Barnes 2008, or Kane & von Braun 2008), and indeed transits were discovered by Barbieri et al. (2007). The relatively long period, along with the large orbital eccentricity of 0.67, presents an interesting opportunity to study the planetary atmospheric response to strongly time-variable heating by the parent star (Langton & Laughlin 2007). However, the long period also presents a challenge to observers. From a given site, there are only 2-3 good opportunities each year to observe a complete transit. Irwin et al. (2008), Narita et al. (2008), and Gillon et al. (2008) observed the photometric transits of Oct. 1, Nov. 12, and Dec. 3, 2007, respectively. They were able to improve upon the precision of the system parameters given originally by Barbieri et al. (2007), but left further scope for improvement through higher-precision photometry.

In this paper we present photometry of the transit of Dec. 25, 2007 based on observations with 4 different telescopes. We also present 10 new measurements of the Doppler shift of the host star, gathered outside of transits. We analyze all of these data to refine the estimates of the system parameters, using similar techniques to those we have applied previously as part of the Transit Light Curve (TLC) project (Holman et al. 2006, Winn et al. 2007) and that were recently applied to a sample of 23 planets by Torres et al. (2008). The observations and data reduction are described in § 2. The data analysis is described in § 3. In § 4, the results of the data analysis are used together with other observed stellar properties and stellar evolutionary models to determine the properties of the star and planet. All of the results are summarized in § 5, and potential future studies are discussed.

2. Observations and Data Reduction

2.1. Out-of-transit radial velocities

Fischer et al. (2007) reported 33 measurements of the radial velocity (RV) of HD 17156 over a time range from January 2006 to February 2007. Of these, 9 velocities were obtained with the Subaru 8m telescope and HDS spectrograph, with a precision of approximately 5 m s^{-1}. The other 24 velocities were based on observations with the Keck I 10m telescope and HIRES spectrograph (Vogt et al. 1994), with a precision of 1-2 m s^{-1}.

To these, we add 10 new Keck/HIRES velocities with 1-2 m s^{-1} precision that were obtained between August 2007 and March 2008. The new data are based on observations with the same telescope, instrument, and setup as the previous Keck observations. In particular we employed an iodine gas absorption cell to calibrate the instrumental profile and wavelength scale. To maintain a consistent signal-to-noise ratio of about 200 per resolution element, we employed the HIRES exposure meter, which uses a pickoff mirror to direct a small fraction of the starlight to a photomultiplier tube and monitors the exposure level as a function of time (Kibrick et al. 2006).

All 34 of the Keck/HIRES velocities were re-measured based on an improved reduction of the raw CCD images and a refined version of the algorithm of Butler et al. (1996), including the use of a new stellar template. (The stellar template, an important ingredient in the deconvolution algorithm of Butler et al. 1996, is an observation of the target star obtained without the iodine cell and with a higher signal-to-noise ratio and higher resolution than the rest of the spectra.) The resulting velocities are given in Table 1. For convenience, this table also includes the Subaru/HDS velocities reported previously. Fig. 1 shows the radial velocities as a function of orbital phase, using the ephemeris derived in § 3.

2.2. Transit photometry

We observed the transit of UT 25 December 2007 (JD 2454459) using telescopes at two different observatories in Arizona: the Fred L. Whipple Observatory (FLWO) and Fairborn Observatory. The Moon was full. The weather was generally clear over both observatories, although there were some light clouds and transparency variations.

At FLWO, we used the 1.2m telescope and Keplercam, a 4096^2 CCD with a $23' \times 23'$ field of view (Szentgyorgyi et al. 2005). The images were binned 2×2, giving a scale of $0\farcs68$ per binned pixel. We obtained 10 s exposures though a z-band filter for 6.5 hr bracketing the predicted midtransit time. The telescope was defocused to avoid significant nonlinearity

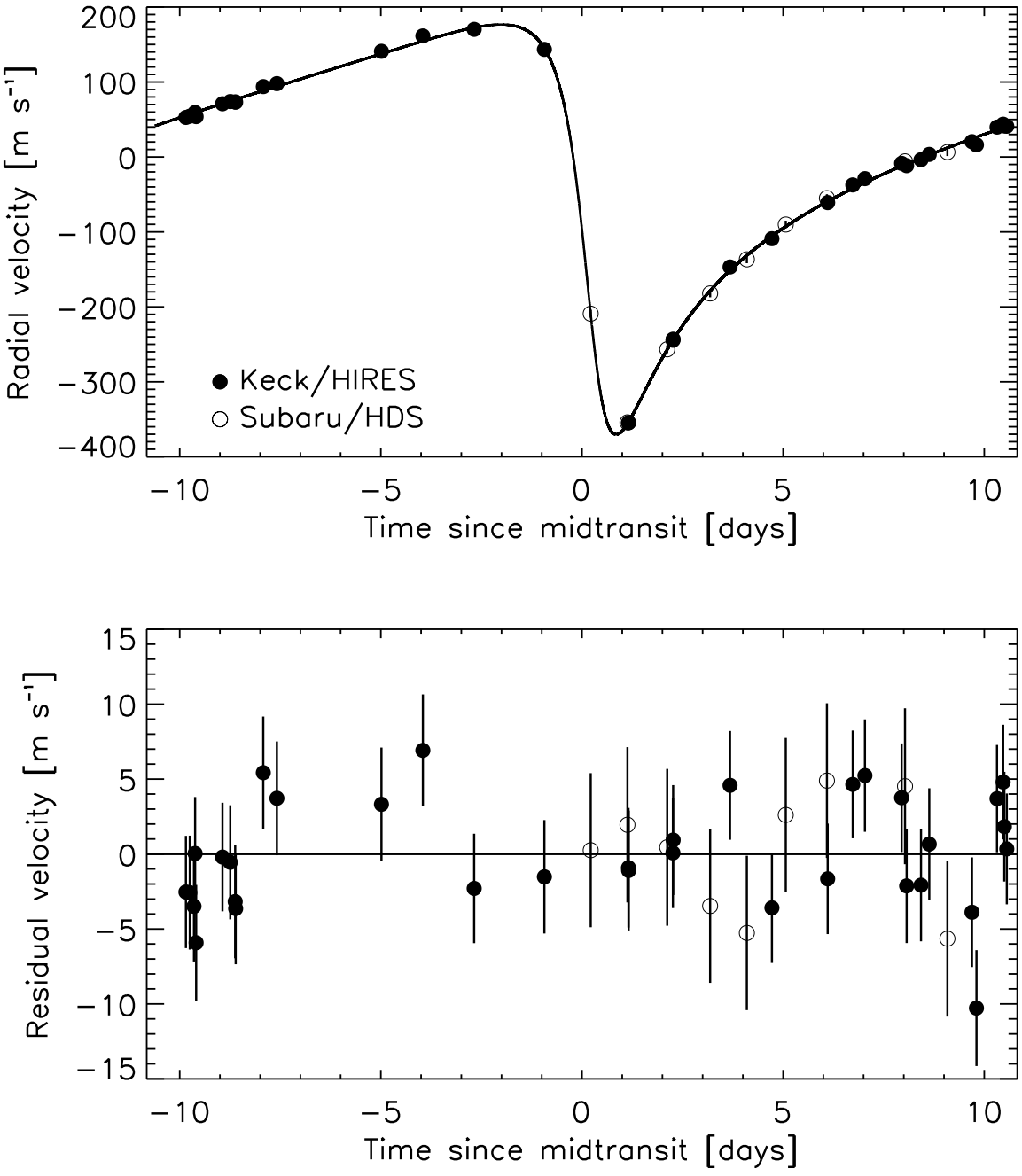

Fig. 1.— Radial velocity (RV) variation of HD 17156. *Top.*—The measured RVs as a function of orbital phase, expressed in days since midtransit. *Bottom.*—Differences between the observed and calculated RVs, using the model described in § 3.3. The root-mean-squared (RMS) residual is 3.8 m s^{-1}.

Table 1. Relative Radial Velocities (RV) of HD 17156

Observatory Code[a]	Heliocentric Julian Date	RV [m s^{-1}]	Measurement Uncertainty [m s^{-1}]
1	2453746.75853	−3.88	1.58
1	2453748.80062	43.59	1.75
1	2453749.79720	54.23	1.70
1	2453750.80399	73.76	1.71
1	2453775.77928	140.82	1.67
1	2453776.80892	161.32	1.55
1	2453779.82980	143.35	1.66
1	2453959.13100	3.25	1.52
1	2453962.06926	55.17	1.41
1	2453963.10508	72.97	1.50
1	2453964.13028	97.69	1.69
1	2453982.03249	39.66	1.12
1	2453983.08599	52.59	1.57
1	2453983.99510	70.80	1.25
1	2453985.00883	93.70	1.57
1	2454023.95452	15.98	1.84
1	2454047.96100	73.25	1.66
1	2454083.90654	−61.08	1.42
1	2454084.83198	−29.07	1.58
1	2454085.86874	−11.78	1.73
1	2454129.92683	20.22	1.35
1	2454130.73184	41.18	1.35
1	2454131.85644	53.68	1.83
1	2454138.76840	170.09	1.33
1	2454319.12775	−8.71	1.25
1	2454336.07987	−146.93	1.27
1	2454337.12124	−109.19	1.40
1	2454339.13050	−37.48	1.17
1	2454427.82655	40.82	1.45
1	2454428.86486	59.19	1.61
1	2454545.72272	−354.79	2.09
1	2454545.72680	−354.61	2.10
1	2454546.82753	−244.68	1.41
1	2454546.83309	−243.35	1.37
2	2454078.01509	−116.60	5.14
2	2454078.92847	−261.56	5.18
2	2454079.91716	−164.10	5.23
2	2454080.98437	−89.57	5.13
2	2454081.89749	−44.08	5.15
2	2454082.86412	2.39	5.14
2	2454083.88785	37.62	5.16
2	2454085.82897	86.67	5.20
2	2454086.88295	99.01	5.20

[a](1) Keck/HIRES. (2) Subaru/HDS.

Note. — The time stamps represent the Heliocentric Julian Date at the time of midexposure.

and saturation, giving a typical full width at half-maximum (FWHM) of stellar images of $4''$ (6 pixels). The time between exposures was 11 s due to readout and reset operations. Autoguiding failures led to pointing drifts of 10 pixels in right ascension and 40 pixels in declination over the course of the night. During the observations the target rose from airmass 1.34 to 1.30 (reaching the meridian at HJD 2454459.67) and then set to airmass 1.64.

We used standard IRAF procedures for overscan correction, trimming, bias subtraction, flat-field division, and aperture photometry of HD 17156 and 32 other stars in the field of view (all necessarily fainter than HD 17156). We created a reference signal by combining the normalized light curves of the different comparison stars, and divided the flux history of HD 17156 by this reference signal. We experimented with different choices for the aperture size, combinations of the comparison stars, and weighting schemes for combining the normalized light curves, aiming to minimize the standard deviation of the out-of-transit portion of the light curve. Best results were obtained when the aperture diameter was 15 pixels and the comparison light curves were weighted by the square root of the mean flux.

At Fairborn Observatory, we used 3 independent telescopes: the T8, T10, and T11 0.8m automated photometric telescopes (APTs). All of the APTs are equipped with two temperature-stabilized EMI 9124QB photomultiplier tubes for measuring photon count rates simultaneously through Strömgren b and y filters. Each telescope nodded back and forth between HD 17156 ($V = 8.17$, $B - V = 0.64$) and the comparison star HD 15784 ($V = 6.64$, $B - V = 0.64$), which was found to be constant in brightness by Fischer et al. (2007). The T8, T10, and T11 APTs obtained 170, 190, and 200 observations of both stars, respectively, over a period 7.2 hours. From these measurements, we computed a total of 560 target-minus-comparison differential magnitudes in each b and y photometric band. The time series was trimmed to 523 points to eliminate bad data taken at the highest airmass. To increase the signal-to-noise ratio in the resulting light curves, we averaged the b and y passbands together, resulting in a synthetic $(b + y)/2$ passband.

The FLWO and APT light curves were corrected for differing airmass extinction between the target star and comparison stars, by fitting the observed magnitudes to a linear function of airmass (see Eqn. 3). The parameters of the linear function were determined simultaneously with the other model parameters, as described in § 3. The extinction-corrected data are given in Table 2, and plotted in Fig. 2, along with the best-fitting model. For the APT data, the standard deviation of the out-of-transit (OOT) data and of the residuals are 0.00214 and 0.00213, respectively. The corresponding figures for the FLWO data are 0.00233 and 0.00206, respectively. For both light curves, the expected photometric precision due only to Poisson noise and scintillation noise (using the empirical formulas of Reiger 1963, Young 1967 and Dravins 1998) is about 50% smaller than the OOT standard deviation, with

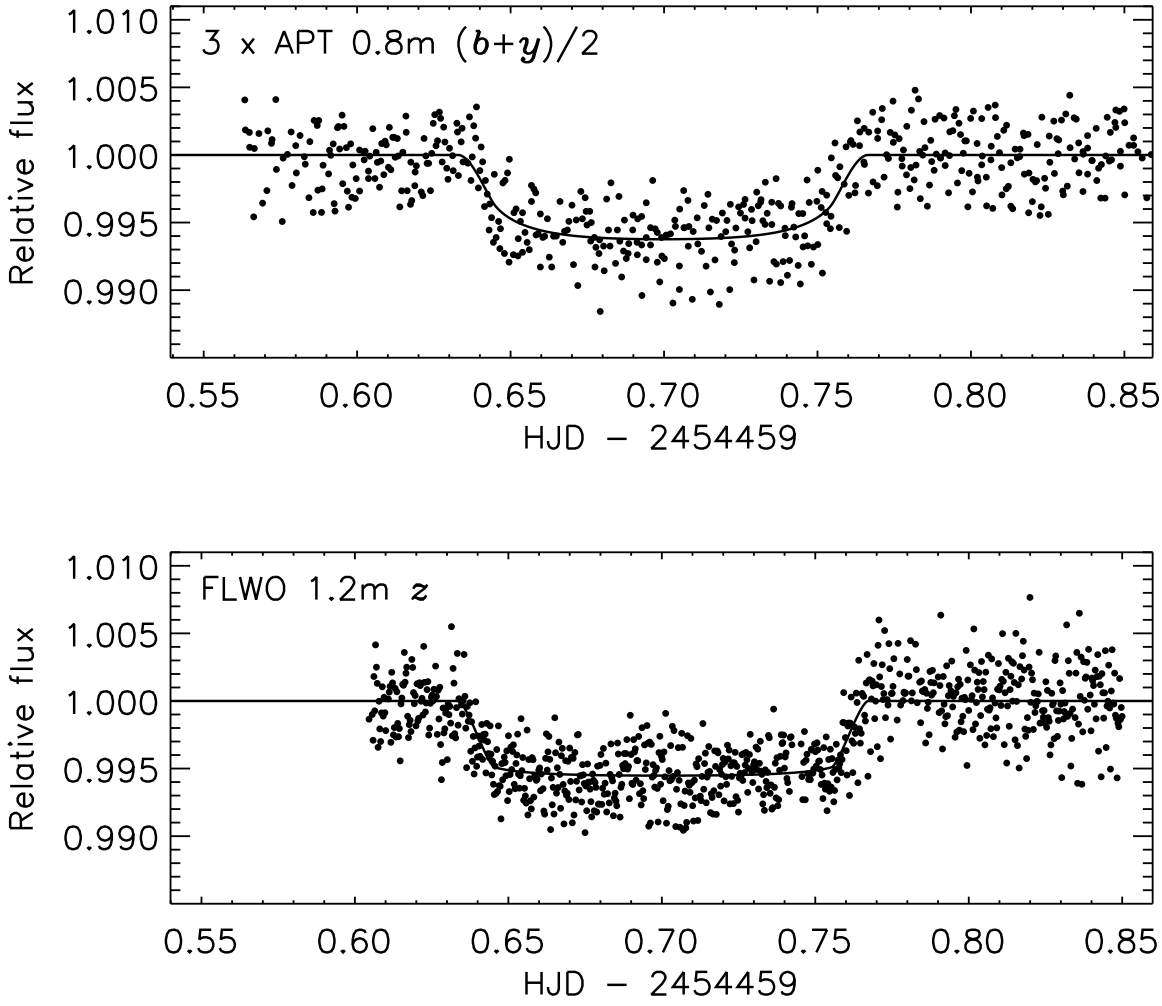

Fig. 2.— Relative photometry of HD 17156 on UT 25 Dec 2007, along with the best-fitting model. *Top.*—Data from the T8, T10, and T11 0.8m automated photometric telescopes at Fairborn Observatory, in the "$(b+y)/2$" band (the Strömgren b and y data were averaged). The median time interval between data points is 43 s. The standard deviation of the out-of-transit (OOT) data and of the residuals are 0.00214 and 0.00213, respectively. *Bottom.*—Data from the Fred L. Whipple 1.2m telescope and Keplercam, in the z band. The median time interval between data points is 24 s. The standard deviation of the OOT data and of the residuals are 0.00233 and 0.00206, respectively.

the dominant contribution arising from scintillation noise. It is possible that the scintillation noise was higher than the empirical and highly approximate formula predicts. It is also likely that there are additional noise sources such as transparency variations beyond the simple dependence on airmass.

3. Analysis of radial-velocity and photometric data

At the heart of our analysis was a simultaneous fit of a parametric model to the new light curves and the available radial-velocity data. In § 3.1 we describe the model and fitting procedures. In § 3.2 we provide more detail about the photometric noise and how it was modeled. In § 3.3 we discuss the determination of midtransit times and a new transit ephemeris. In § 4 we explain how the data analysis was integrated with stellar evolutionary models to determine the final system parameters.

3.1. Joint radial velocity and photometric analysis

The model is based on a two-body Keplerian orbit, with the loss of light during transits given by the formulae of Mandel & Agol (2002). The orbit is parameterized by the semi-amplitude (K), period (P), midtransit time (T_c)[1], inclination (i), eccentricity (e), and argument of pericenter (ω). The coordinate system is chosen such that $i < 90^\circ$ and the longitude of nodes is zero.

Additional parameters relevant to the photometric data are the planet-to-star radius ratio ($R_p/R_\star$), the semimajor axis in units of the stellar radius ($a/R_\star$), and the limb-darkening coefficients (u_1 and u_2) for each light curve. We assumed a quadratic limb-darkening law,

$$\frac{I_\mu}{I_1} = 1 - u_1(1-\mu) - u_2(1-\mu)^2, \tag{1}$$

where μ is the cosine of the angle between the line of sight and the normal to the stellar surface, and I_μ is the specific intensity. In many studies of transiting planets, the limb-darkening coefficients are often held fixed at values deemed appropriate for the host star,

[1]Since the orbit of HD 17156b is highly eccentric, the definition of T_c requires some care. Here we define it as the time when the projected planet-star separation is smallest, which is also the time of minimum light for a limb-darkened star. This is to be distinguished from other possible definitions, such as the halfway point between first and last contact, or the moment when the true anomaly f of the planetary orbit is equal to $\pi/2 - \omega$.

based on stellar-atmosphere models. However, when the data are sufficiently precise it is preferable to fit for the coefficients, as recently emphasized by Southworth (2008). This is because the model atmospheres might be wrong, and at least are uncertain to some degree. Neglecting this uncertainty leads to underestimated errors in all parameters that are covariant with the limb-darkening coefficients, namely $R_p/R_\star$, $R_\star/a$, and i. For this study we allowed u_1 and u_2 to vary freely subject only to the conditions $u_1 + u_2 < 1$ (nonnegative intensity at the limb), $u_1 + u_2 > 0$ (fainter at the limb than the center), and $u_1 > 0$ (maximum intensity at the center). It proved advantageous to perform the fit using the linear combinations

$$v_1 = u_1 + \frac{7}{5}u_2, \quad v_2 = -\frac{7}{5}u_1 + u_2, \tag{2}$$

because v_1 and v_2 have nearly uncorrelated errors (for further discussion, see Pál 2008).

The model also has 6 nuisance parameters. For each of the two RV data sets there is an additive constant velocity (γ_K for Keck/HIRES and γ_S for Subaru/HDS). For each of the two light curves there are the parameters m_0 and k of the differential extinction correction,

$$m_{\rm cor} = m_{\rm obs} + m_0 + kz, \tag{3}$$

where $m_{\rm obs}$ is the observed magnitude, $m_{\rm cor}$ is the corrected magnitude, and z is the airmass.

All together there were 18 parameters: K, P, T_c, i, e, ω, $R_p/R_\star$, $a/R_\star$, an additive velocity for each of two RV data sets, two limb-darkening coefficients u_1 and u_2 for each of two bandpasses, and two parameters m_0 and k for each of two bandpasses to describe the correction for differential airmass extinction. The fitting statistic was

$$\chi^2 = \chi^2_F + \chi^2_V + \chi^2_T, \tag{4}$$

with the terms defined as follows. The first term is based on the fit to the photometric data:

$$\chi^2_F = \sum_{i=1}^{1372} \left[\frac{f_i({\rm obs}) - f_i({\rm calc})}{\sigma_{f,i}} \right]^2, \tag{5}$$

where f_i(obs) is the ith measured flux (photometric data point), f_i(calc) is the calculated flux given a particular choice of model parameters, and $\sigma_{f,i}$ is the uncertainty in the ith measured flux. The choice of $\sigma_{f,i}$ is nontrivial and is discussed in § 3.2. Here we simply state our choice to take $\sigma_{f,i}$ to be a constant for each light curve given by $\sigma_{f,i} = \beta\sigma_{\rm res}$, where $\sigma_{\rm res}$ is the standard deviation of the flux residuals, and $\beta \geq 1$ is a factor intended to account for time-correlated errors. For the APT light curve, $\sigma_{\rm res} = 0.00213$ and $\beta = 1.03$, giving an effective uncertainty per point of 0.0022. For the FLWO light curve, $\sigma_{\rm res} = 0.00207$ and $\beta = 1.28$, giving an effective uncertainty per point of 0.0026.

The second term in Eqn. (4) is based on the fit to the RV data:

$$\chi^2_V = \sum_{i=1}^{43} \left[\frac{V_i(\mathrm{obs}) - V_i(\mathrm{calc})}{\sigma_{V,i}} \right]^2, \tag{6}$$

where V_i(obs) and V_i(calc) are the ith observed and calculated RVs, and $\sigma_{V,i}$ is the corresponding uncertainty. For $\sigma_{V,i}$, we used the quadrature sum of the measurement uncertainty given in Table 1 and a constant $\sigma_{V,0} = 3.4$ m s^{-1} intended to account for stellar "jitter," excess noise that is usually attributed to motions of the stellar photosphere. This choice resulted in a reduced χ^2_V of unity when fitting the RV data only, and it is consistent with observations of other stars of similar type (Wright 2005).

The third term in Eqn. (4) is an *a priori* constraint enforcing the transit ephemeris that is derived in § 3.3. Specifically,

$$\chi^2_T = \left[\frac{P\ (\mathrm{days}) - 21.21688}{0.00044} \right]^2 + \left[\frac{T_c\ (\mathrm{HJD}) - 2,454,459.69987}{0.00045} \right]^2. \tag{7}$$

The central values of P and T_c, and their uncertainties, are derived in § 3.3 based on observations of 5 different transits spanning 106 days. They are more precise than could be derived internally from only the RV data, the APT data, and the FLWO data that are fitted here; hence during this step we treated P and T_c as externally measured quantities. Since the transit ephemeris is based in part on the midtransit times of the APT and FLWO light curves, we used an iterative procedure: first, a previously published ephemeris was used in Eqn. (7); second, the midtransit times based on the APT and FLWO light curves were determined as in § 3.3; and third, the ephemeris was re-derived and used in the next iteration of the fit to the RV and photometric data. Further iterations were performed but made no appreciable difference in the results.

We used a Markov Chain Monte Carlo (MCMC) algorithm to estimate the best-fitting model parameters and their uncertainties (see, e.g., Appendix A of Tegmark et al. 2004). This algorithm creates a sequence of points (a "chain") in parameter space by iterating a jump function, which in our case was the addition of a Gaussian random deviate to a randomly-selected single parameter. After this operation, if the new point has a lower χ^2 than the previous point, the "jump" is executed: the new point is added to the chain. If not, then the jump is executed with a probability proportional to $\exp(-\Delta\chi^2/2)$. If the jump is not executed, the current point is repeated in the chain. The sizes of the random deviates are set to values for which ∼40% of jumps are executed. After creating multiple chains to check for mutual convergence, and trimming off the initial segments to eliminate artifacts of the initial condition, the density of the chain's points in parameter space is taken to be the joint *a posteriori* probability distribution of the parameter values. Probability distributions

for individual parameters are created by marginalizing over all other parameters. For each parameter we report the mode of the distribution and the 68.3% confidence limits, defined by the 15.85% percentile and the 84.15% percentile in the cumulative distribution.

The results are given in Table 3, with the designation A in the last column. The entries designated B are those that are drawn from other works and are repeated here for convenience. The entries designated C are based on a synthesis of our modeling results and theoretical models of stellar evolution, as discussed in § 4. The results for the limb-darkening parameters are given separately, in Table 4.

3.2. Photometric noise analysis

Deriving reliable uncertainties in the system parameters requires a realistic treatment of the photometric noise. In this work, as in others, we have based our analysis on a χ^2 statistic that implicitly treats the noise as independent and identically-distributed Gaussian random variables added to each datum. This is because simple and fast statistical methods are applicable in that case, and because there is no clear alternative. Unfortunately, precise photometry is often plagued with time-correlated ("red") noise, which is probably responsible for the frequent disagreements between reported values of photometric parameters in the literature. It is advisable to attempt to justify the common assumption of independent Gaussian noise, or at least to gain some understanding of the limitations of that assumption.[2].

To investigate the noise in our light curves, we performed some tests on the residuals. The top two panels in Fig. 3 show the residuals for the two independent light curves. The second row shows histograms of the residuals, which are approximately Gaussian. The third row shows the autocorrelation of the residuals as a function of the lag,

$$A(l) = \frac{\sum_{i=0}^{N-l-1}(r_i - \bar{r})(r_{i+l} - \bar{r})}{\sum_{i=0}^{N-1}(r_i - \bar{r})^2}, \tag{8}$$

where N is the number of data points, r_i is the ith residual flux (measured flux minus calculated flux) and $\bar{r}$ is the mean residual flux. The autocorrelations are $\lesssim$0.1. The fourth row shows the Allan deviation $\sigma_A(l)$ of the residuals, where σ_A is defined by (Allan 1964;

[2]In this vein we quote an email from G. Kovacs: "Identifying the 'red noise component' (whatever it means) in a single realization of a rather limited time series (such as photometric followup data) is a mission impossible."

Thompson, Moran, & Swensen 2001)

$$\sigma_A^2(l) = \frac{1}{2(N+1-l)} \sum_{n=0}^{N-2l} \left[\frac{1}{l} \sum_{m=0}^{l} (r_{n+m} - r_{n+l+m}) \right]^2 , \tag{9}$$

where N is the number of data points, r_i denotes the ith residual, and l is the lag. The Allan deviation is commonly used in the time metrology literature to assess $1/f$ noise. The solid lines show the dependence $\sigma_A \propto l^{-1/2}$ that is expected of white Gaussian noise. The data fall close to these lines. The bottom row of panels shows the standard deviation of the time-binned residuals, as a function of the number of data points per bin. Specifically, we averaged the residuals into m bins of n points and calculated the standard deviation σ_n of the binned residuals. In the absence of red noise, one would expect

$$\sigma_n = \frac{\sigma_1}{n^{1/2}} \left(\frac{m}{m-1} \right)^{1/2} , \tag{10}$$

but in reality σ_n is larger than this expression by a factor β. In general β depends on m but the dependence is weak. For bin sizes ranging from 10-30 min (the most important timescale of the transit light curve) the mean value of β is 1.03 for the APT light curve and 1.28 for the FLWO light curve. Apparently the APT residuals average down as one would expect of white noise, while the FLWO residuals are correlated to some degree.

As stated above, our χ^2-based method is strictly appropriate only for uncorrelated errors. One might imagine modifying the definition of χ_F^2 to employ the full covariance matrix of the errors rather than assuming independent errors. However, given that there is little structure in the autocorrelation functions to provide guidance on how to model the covariance matrix, and that the correlations seem small, we account for correlated noise in a simple and approximate fashion: we assign a photometric error bar of $\sigma_{f,i} = \beta\sigma_{\rm res}$ to each data point, where $\sigma_{\rm res}$ is the standard deviation of the residuals. The choice $\beta = 1$ is essentially equivalent the common procedure of assuming equal errors for all data points and scaling the error bars such that $\chi^2/N_{\rm dof} = 1$. We used $\beta = 1.03$ for the APT data and $\beta = 1.28$ for the FLWO data.

3.3. Midtransit times

Measurements of midtransit times are important for refining the transit ephemeris and thereby enabling accurate predictions for future observations, and also for searching for satellites and additional planets via the method of Holman & Murray (2005) and Agol et al. (2005). We determined the midtransit time from each light curve using 3 different methods

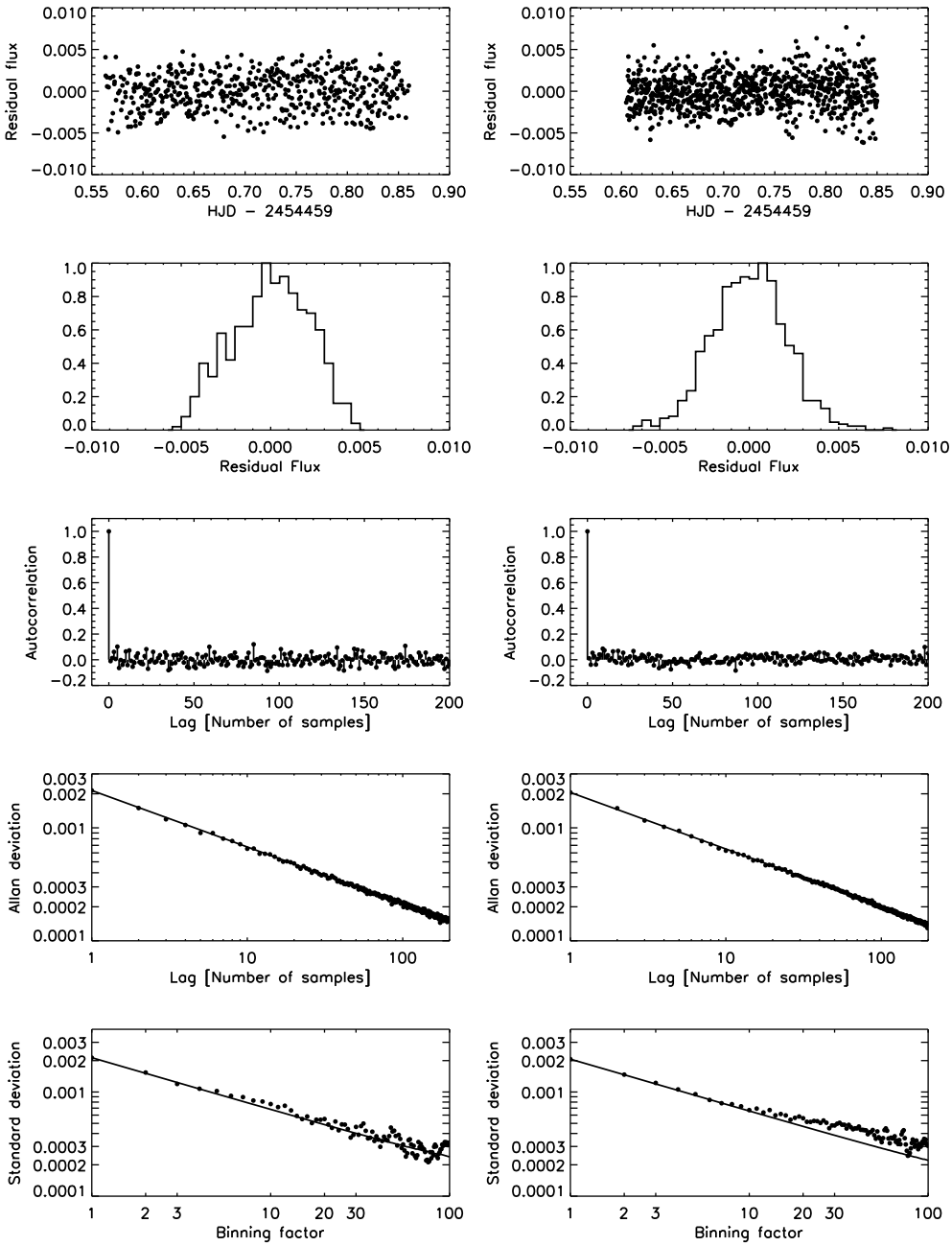

Fig. 3.— Photometric noise analysis. The left column applies to the APT $(b+y)/2$ data, and the right column applies to the FLWO 1.2m z data. *First row.*—Residuals from the best-fitting model (observed−calculated). *Second row.*—Histogram of the residuals. *Third row.*—Autocorrelation of the residuals as a function of the lag. *Fourth row.*—Allan deviation of the residuals, as a function of the lag. The straight line shows the $l^{-1/2}$ dependence that is expected of white Gaussian noise. *Fifth row.*—Standard deviation of time-binned residuals, as a function of the number of data points per bin. The straight line shows the expectation for white Gaussian noise (see Eqn. 10).

to check for consistency: the MCMC algorithm described in § 3.1, and two different bootstrap analyses described below. All of these methods rely on the photometric transit model and the computation of χ^2_F. Besides T_c, the only other variable parameters were the slope (k) and offset (m_0) of the differential extinction correction. These were the only other parameters covariant with the midtransit time. All other parameters needed to specify the transit model were held fixed at the best-fitting values.

The first bootstrap method was "random draws with replacement" (Press et al. 1992, p. 689). It involves minimizing χ^2_F as a function of the parameters for 10^4 synthetic data sets, each of which has the same number of data points as the real data. Each entry in a synthetic data set is a datum (a time stamp and relative flux) drawn randomly from the real data set, with repetitions allowed. Thus, a substantial fraction of the entries in each synthetic data set are duplicated at least once and receive greater weight in χ^2_F sum. The idea is to estimate the noise properties of the data using the observed data values themselves, rather than choosing models for the underlying physical process and for the noise. However, an underlying assumption is that the errors are uncorrelated and identically distributed. The distribution of results for T_c is taken to be the probability density for the midtransit time.

The second bootstrap method was "residual permutation." It is similar to the method just described but the synthetic data sets are created differently. The residuals of the best-fitting model are added back to the model light curve after performing a cyclic permutation of their time indices. With N data points, one may create $N-1$ synthetic data sets in this manner. Another $N-1$ may be created by inverting the time order of the residuals and then performing cyclic permutations. The idea is again to use the data themselves to estimate the noise properties, but this time without assuming that the errors are uncorrelated. The correlations between residuals at different times are preserved. The distribution of results for T_c is taken to be the probability density for the midtransit time. A disadvantage of this method is that only $2(N-1)$ realizations can be generated without further assumptions, and therefore the distribution is relatively noisy.

The results from all 3 methods are given in Table 5. As before, the quoted values are the modes of the probability distributions and the quoted error bars range from the 15.85% percentile to the 84.15% percentile. The distributions are symmetric in all cases, and are nearly Gaussian for the MCMC and random-draws methods. The residual-permutation method produced distributions with broader wings than a Gaussian function. For each light curve, the results from all 3 methods are in agreement within 0.15σ, where σ is the error in the MCMC method. The bootstrap method gave the smallest error bars, as one might expect, given that the bootstrap method ignores correlated noise. (The bootstrap-derived error bar is smaller than the MCMC-derived error bar by approximately the "red noise"

factor β.) In what follows, we adopt the MCMC results for concreteness and for consistency with our previous analyses. The error bars on the midtransit times derived from the FLWO and APT light curves are 1.1 min and 0.9 min, and the difference between the results is 1.0 min. This level of agreement is a consistency check on the accuracy of our error bars.

We fitted a linear ephemeris, $T_c[E] = T_c[0] + EP$, to all of the midtransit times at our disposal: namely, the APT and FLWO midtransit times presented in this paper, and the 4 different midtransit times reported by Barbieri et al. (2007), Gillon et al. (2008), Irwin et al. (2008), and Narita et al. (2008). For convenience, all of the midtransit times are given in Table 6. The results were

$$T_c[0] = 2,454,459.69987 \pm 0.00045 \text{ [HJD]}, \quad (11)$$

$$P = 21.21688 \pm 0.00044 \text{ days}. \quad (12)$$

The fit gives $\chi^2 = 1.99$ with 4 degrees of freedom, suggesting that a constant period is consistent with the available data. A plot of the timing residuals (observed−calculated midtransit times) is shown in Fig. 4. There are no obvious anomalies at the level of a few minutes.

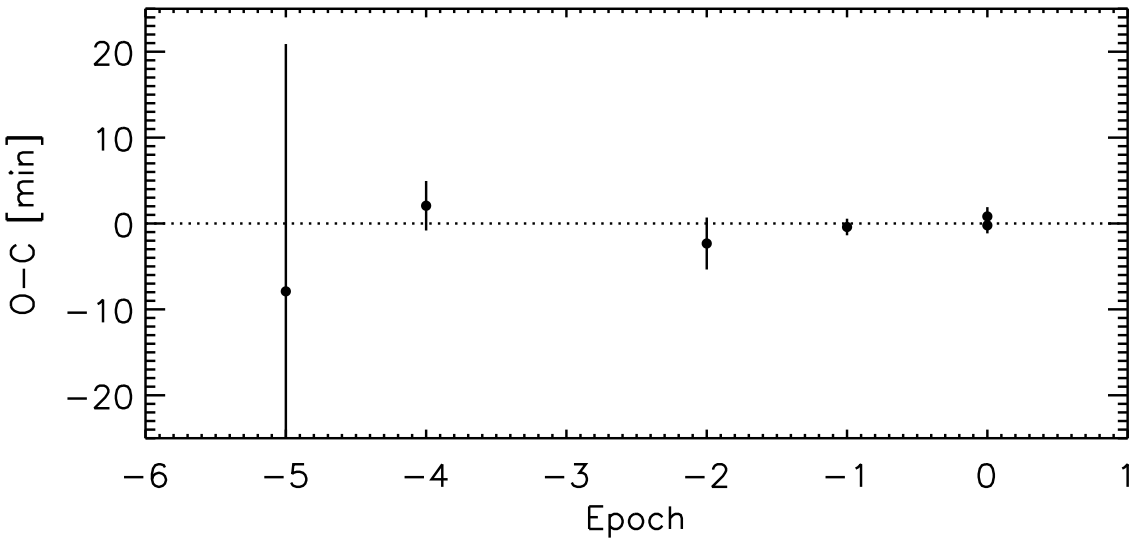

Fig. 4.— Transit timing residuals for HD 17156b. The calculated times, using the ephemeris given in Eqns. (11,12), have been subtracted from the observed times.

4. Theoretical isochrone fitting

The RV and photometric data do not uniquely determine the masses and radii of the planet and the star. Some external information about the star or the planet must be introduced to break the fitting degeneracies $M_p \propto M_\star^{2/3}$ and $R_p \propto R_\star \propto M_\star^{1/3}$ (see, e.g., Winn 2008). We broke these degeneracies by requiring consistency between the observed properties of the star, the stellar mean density $\rho_\star$ that can be derived from the photometric parameter $a/R_\star$ (Seager & Mallen-Ornelas 2003, Sozzetti et al. 2007), and theoretical models of stellar evolution. The inputs were $T_{\rm eff} = 6079 \pm 80$ K and [Fe/H] $= +0.24 \pm 0.05$ (from Fischer et al. 2007 but with enlarged error bars, as per Torres et al. 2008), the absolute magnitude[3] $M_V = 3.80 \pm 0.12$, the stellar mean density $\rho_\star = 0.589^{+0.066}_{-0.103}$ g cm^{-3} derived from the results for the $a/R_\star$ parameter, and the Yonsei-Yale (Y^2) stellar evolution models by Yi et al. (2001) and Demarque et al. (2004). We computed isochrones for the allowed range of metallicities, and for stellar ages ranging from 0.1 to 14 Gyr. For each stellar property (mass, radius, and age), we took a weighted average of the points on each isochrone, in which the weights were proportional to $\exp(-\Delta\chi^2_\star/2)$ with

$$\chi^2_\star = \left[\frac{\Delta[\mathrm{Fe/H}]}{\sigma_{[\mathrm{Fe/H}]}}\right]^2 + \left[\frac{\Delta T_{\rm eff}}{\sigma_{T_{\rm eff}}}\right]^2 + \left[\frac{\Delta\rho_\star}{\sigma_{\rho_\star}}\right]^2 + \left[\frac{\Delta M_V}{\sigma_{M_V}}\right]^2 . \quad (13)$$

Here, the Δ quantities denote the deviations between the observed and calculated values at each point. The asymmetric error bar in $\rho_\star$ was taken into account by using different values of $\sigma_{\rho_\star}$ depending on the sign of the deviation. The weights were further multiplied by a factor taking into account the number density of stars along each isochrone, assuming a Salpeter mass function. We used the same code as Torres et al. (2008) and refer the reader to that paper for further details.

Through this analysis, we found $M_\star = 1.263^{+0.035}_{-0.047}\ M_\odot$, $R_\star = 1.446^{+0.099}_{-0.067}\ R_\odot$, and a stellar age of $3.18^{+0.52}_{-0.68}$ Gyr. The corresponding planetary mass and radius were obtained by merging the results for the stellar properties with the parameters determined in our analysis of the RV and photometric data. The results are $M_p = 3.212^{+0.069}_{-0.082}\ M_{\rm Jup}$ and $R_p = 1.023^{+0.070}_{-0.055}\ R_{\rm Jup}$. These values are also given in Table 3, along with the values for some other interesting parameters that can be derived from the preceding results.

As a consistency check, we computed the implied stellar surface gravity and its uncertainty based on our analysis, finding $\log g = 4.219^{+0.033}_{-0.055}$ where g is in cm s^{-2}. This

[3]The quoted M_V is based on the transformation of Tycho-2 apparent magnitudes (Høg et al. 2000) to the Johnson V band, giving $V = 8.172 \pm 0.012$, and the Hipparcos parallax of $\pi = 13.34 \pm 0.72$ mas (van Leeuwen 2007). We have assumed zero reddening.

agrees with the spectroscopic determination of surface gravity, $\log g = 4.29 \pm 0.06$ (Fischer et al. 2007), based on an analysis of the widths of pressure-sensitive lines in the optical spectrum. Since the error bars on the two results are comparable, one might be tempted to use the spectroscopic $\log g$ as a further constraint on the stellar properties. We did not take this approach out of concern that the spectroscopic determination is more complex and liable to underestimation of the error (see, e.g., Winn et al. 2008).

5. Discussion

5.1. Summary and comparison with previous results

We have presented photometry of a transit of HD 17156b, and 10 additional measurements of the radial velocity of the host star. We have analyzed the data along with the other observed stellar properties to refine the estimates of the basic system parameters. For many of the parameters, our results are more precise than those reported previously, despite some aspects of the previous analyses that may have caused the quoted error bars to be unrealistically small. Specifically, none of the previous analyses allowed for any uncertainty in the limb-darkening law, and neither Barbieri et al. (2007) nor Irwin et al. (2008) attempted to quantify the effect of time-correlated noise. Another improvement in our analysis was the integration of the data analysis with stellar evolution models to make full use of the information in the light curve and arrive at a self-consistent solution.

Our result for the stellar mass, $M_\star = 1.263^{+0.035}_{-0.047}\ M_\odot$, agrees with the previous determination of $1.2 \pm 0.1\ M_\odot$ by Fischer et al. (2007) and improves on the precision. Our result for the stellar radius, $1.446^{+0.099}_{-0.067}\ R_\odot$, agrees with the Fischer et al. (2007) estimate of $1.470 \pm 0.085\ R_\odot$. The essential difference between the two analyses is that we made use of the photometric determination of $\rho_\star$ while Fischer et al. (2007) used the spectroscopic determination of $\log g$. As for the planet, our result of $1.023^{+0.070}_{-0.055}\ R_{\rm Jup}$ is very similar to the value $1.01 \pm 0.09\ R_{\rm Jup}$ found by Irwin et al. (2008). This should be interpreted as an agreement between the measured transit depths, and not necessarily the other light curve parameters, because Irwin et al. (2008) did not fit for the $a/R_\star$ parameter. Instead they used an external constraint on that parameter based on the work by Fischer et al. (2007). Gillon et al. (2008) also found the same transit depth, but a smaller value of $a/R_\star$ and therefore larger values of $R_\star$ and R_p (by about 1σ, where σ is the error quoted by Gillon et al. 2008). Our result for R_p is approximately 3 times more precise.

The results for the limb-darkening coefficients, given in Table 4, show that the darkening is greater in the $(b+y)/2$ band than in the z band, as expected. The values of the coefficients

themselves are poorly constrained and the errors are highly correlated, making it difficult to compare to specific theoretical predictions. For the z band, interpolation of the tables of Claret (2004) gives a prediction of $u_1 = 0.17$ and $u_2 = 0.35$, which is just outside the 1σ range of our results. The data favor a less limb-darkened star. The tables of Claret (2000) give $u_1 = 0.52$ and $u_2 = 0.28$ for the b band, and $u_1 = 0.39$ and $u_2 = 0.33$ for the y band. Either set of coefficients is compatible with the loose bounds provided by the APT data.

5.2. Comparison with theoretical models

A primary goal of precise transit observations is to compare the observed planetary properties with theoretical models of the planet's interior structure. For example, a persistent theme in this field is that at least a few planets have radii that are "too large" by the standards of theoretical models of solar-composition giant planets, even after accounting for the intense stellar heating and selection effects (see Burrows et al. 2007 for a recent discussion). Other planets are so small that the models fit only when the composition is altered to be much richer in heavy elements than the Sun, a possible indication of the dense interior cores that are expected according to the core-accretion theory of planet formation (see, e.g., Sato et al. 2005).

Bodenheimer et al. (2003) give predictions for the radii of giant planets as a function of the age, mass, and time-averaged equilibrium temperature of the planet, defined as

$$T_{\rm eq} = \left[\frac{(1-A)L_\star}{16\pi\sigma a^2(1+e^2/2)^2}\right]^{1/4} = \ (783\ {\rm K})\ (1-A)^{1/4}, \tag{14}$$

where A is the Bond albedo, $L_\star$ is the stellar luminosity, σ is the Stefan-Boltzmann constant, a is the semimajor axis, and e is the eccentricity. In the latter equality we have evaluated $T_{\rm eq}$ for HD 17156b using the results given in Table 3. As long as the albedo is not very close to unity, Bodenheimer et al. (2003) predict a planetary radius of 1.10 $R_{\rm Jup}$ for a solar composition at 4.5 Gyr. They also considered enriching the solar composition by 40 $M_\oplus$ of additional heavy elements (4% of the total mass) and found that the radius decreases by less than 1%.

Fortney et al. (2007) have presented theoretical models parameterized by mass, age, and an effective orbital distance, defined as the distance from the Sun where a hypothetical planet on a circular orbit would receive the same time-averaged flux as the actual planet,

$$d_\oplus = a(1+e^2/2)\left(\frac{L_\star}{L_\odot}\right)^{1/2} = \ 0.13\ {\rm AU}, \tag{15}$$

where again we have evaluated the expression as appropriate for HD 17156b. Fortney et al. (2007) also predicted 1.10 $R_{\rm Jup}$ for a solar composition at 4.5 Gyr, decreasing to 1.02 $R_{\rm Jup}$ when 100 $M_\oplus$ of solar-composition material (10% of the total mass) is replaced by a heavy-element "core." This would provide a good match to the observed radius of 1.023 $R_{\rm Jup}$.

We conclude from these comparisons, as did Irwin et al. (2008), that HD 17156b is smaller than a theoretical giant planet of solar-composition, and that this may be an indication of heavy-element enrichment. Heavy-element enrichment is expected according to the core-accretion model of planet formation (Mizuno 1980, Pollack et al. 1996). There is evidence for such enrichment in Jupiter and Saturn, with Jupiter in particular consisting of 3-15% heavy elements (Guillot 2005). One should be wary of over-interpretation, given that our measurement of R_p differs from 1.1 $R_{\rm Jup}$ by only 1.1 times the measurement uncertainty. However, there are some known factors that would increase the theoretical radius and thereby enlarge the discrepancy at least slightly: the fiducial radius calculated by Bodenheimer et al. (2003) and Fortney et al. (2007) refers to a higher pressure (smaller radius) than the transit-measured radius (Burrows et al. 2003); the models do not take into account tidal heating and consequent inflation due to the nonzero eccentricity (Liu et al. 2008); and the age of the system is estimated to be 3 Gyr, younger than the 4.5 Gyr age for which the models were calculated.

5.3. The spin-orbit angle, and the probability of secondary eclipses

One parameter that we have not improved on, but that deserves mention, is the angle between the stellar spin axis and the orbital axis. One might expect the axes to be well-aligned, given that the star and planet formed from a common disk and given the good alignment observed in the Solar system. Then again, by the same logic the orbit should be circular, and it is not. A lower limit on the angle between the spin and orbital axes can be derived by monitoring the apparent Doppler shift throughout a transit, exploiting the Rossiter-McLaughlin (RM) effect (see, e.g., Queloz et al. 2000, Winn et al. 2005). Using this technique, Narita et al. (2008) found that the angle between sky projections of the two axes is $\lambda = 62 \pm 25$ deg, a 2.5σ misalignment. Cochran et al. (2008) presented two different data sets giving $\lambda = 4.5 \pm 15.6$ deg and $\lambda = -32.4 \pm 25.2$ deg, and concluded that the data are consistent with good alignment. Unfortunately, our new data alone do not allow for significant progress on this issue, because the limiting errors are in the precision of the RM data, which we have not improved in this study. Further spectroscopic observations are warranted.

Another important angle is the orbital inclination with respect to the sky plane. If the

orbit is oriented close enough to edge-on, then the planet will be periodically eclipsed by the parent star. Observations of such secondary eclipses would reveal the planetary albedo or thermal emission from the planet, depending upon the observing bandpass. In addition, infrared observations could help to understand the radiative dynamics of the planetary atmosphere, as emphasized by Barbieri et al. (2007). To check whether secondary eclipses are likely to occur, we used our MCMC results to compute the *a posteriori* probability distribution for the impact parameter at superior conjunction,

$$b_{\rm II} = \frac{a\cos i}{R_\star}\left(\frac{1-e^2}{1-e\sin\omega}\right). \tag{16}$$

We find the probability for secondary eclipses ($b_{\rm II} < 1 + R_p/R_\star$) to be 18%. The probability for complete eclipses, or occultations ($b_{\rm II} < 1 + R_p/R_\star$), is 15%. These odds are better than those found by Irwin et al. (2008), which were 6.9% and 9.2%. Gillon et al. (2008) found the probability of occultations to be 0.04%. Presumably this significant difference is attributable to our finding of a more edge-on orbit ($i = 86.2^{+2.1}_{-0.8}$ deg, as opposed to $85.5^{+1.9}_{-1.2}$ deg from Gillon et al. (2008). Our error bars for i are no smaller than those reported previously because the achievable error in i worsens rapidly as i approaches 90 deg (Carter et al. 2008). To help in planning observations, we have used our results to predict the timing of the events, as well as the quantity $(R_p/d_{\rm II})^2$ (where $d_{\rm II}$ is the star-planet distance at superior conjunction) which sets the amplitude of the reflected-light signal from the planet. The results for this latter parameter are conditioned on the assumption that secondary eclipses do indeed occur. The results are given in Table 7. With a bit of luck, HD 17156b will be eclipsed and give observers another gift.

We are grateful to the referee, Kaspar von Braun, for a timely and detailed critique. This research was partly supported by Grant No. 2006234 from the United States-Israel Binational Science Foundation (BSF). Partial support also came from NASA Origins grants NNG06GH69G (to M.J.H.) and NNG04LG89G (to G.T.). G.W.H. acknowledges support from NASA, NSF, and the State of Tennessee through its Centers of Excellence program. J.A.J. is a National Science Foundation Astronomy and Astrophysics Postdoctoral Fellow with support from the NSF grant AST-0702821. KeplerCam was developed with partial support from the Kepler Mission under NASA Cooperative Agreement NCC2-1390 and the Keplercam observations described in this paper were partly supported by grants from the Kepler Mission to SAO and PSI.

REFERENCES

Agol, E., Steffen, J., Sari, R., & Clarkson, W. 2005, MNRAS, 359, 567

Allan, D. W. 1966, Proc. IEEE, 54, 221

Barbieri, M., et al. 2007, A&A, 476, L13

Barnes, J. W. 2007, PASP, 119, 986

Bodenheimer, P., Laughlin, G., & Lin, D. N. C. 2003, ApJ, 592, 555

Burke, C. J. 2008, ApJ, 679, 1566

Burrows, A., Sudarsky, D., & Hubbard, W. B. 2003, ApJ, 594, 545

Burrows, A., Hubeny, I., Budaj, J., & Hubbard, W. B. 2007, ApJ, 661, 502

Butler, R. P., Marcy, G. W., Williams, E., McCarthy, C., Dosanjh, P., & Vogt, S. S. 1996, PASP, 108, 500

Carter, J. A., Yee, J. C., Eastman, J., Gaudi, B. S., & Winn, J. N. 2008, ArXiv e-prints, 805, arXiv:0805.0238

Charbonneau, D., Brown, T. M., Burrows, A., & Laughlin, G. 2007, Protostars and Planets V, 701

Claret, A. 2000, A&A, 363, 1081

Claret, A. 2004, A&A, 428, 1001

Cochran, W. D., Redfield, S., Endl, M., & Cochran, A. L. 2008, ApJ, 683, L59

Demarque, P., Woo, J.-H., Kim, Y.-C., & Yi, S. K. 2004, ApJS, 155, 667

Dravins, D., Lindegren, L., Mezey, E., & Young, A. T. 1998, PASP, 110, 610

Fischer, D. A., et al. 2007, ApJ, 669, 1336

Fortney, J. J., Marley, M. S., & Barnes, J. W. 2007, ApJ, 659, 1661

Gillon, M., Triaud, A. H. M. J., Mayor, M., Queloz, D., Udry, S., & North, P. 2008, A&A, 485, 871

Guillot, T. 2005, Annual Review of Earth and Planetary Sciences, 33, 493

Høg, E., et al. 2000, A&A, 355, L27

Holman, M. J., & Murray, N. W. 2005, Science, 307, 1288

Holman, M. J., et al. 2006, ApJ, 652, 1715

Irwin, J., et al. 2008, ApJ, 681, 636

Kane, S. R., & von Braun, K. 2008, arXiv:0808.1890

Kibrick, R. I., Clarke, D. A., Deich, W. T. S., & Tucker, D. 2006, Proc. SPIE, 6274, 62741U

Langton, J., & Laughlin, G. 2008, ApJ, 674, 1106

Liu, X., Burrows, A., & Ibgui, L. 2008, ArXiv e-prints, 805, arXiv:0805.1733

Mandel, K., & Agol, E. 2002, ApJ, 580, L171

Mizuno, H. 1980, Progress of Theoretical Physics, 64, 544

Narita, N., Sato, B., Ohshima, O., & Winn, J. N. 2008, PASJ, 60, L1

Pál, A. 2008, ArXiv e-prints, 805, arXiv:0805.2157

Pollack, J. B., Hubickyj, O., Bodenheimer, P., Lissauer, J. J., Podolak, M., & Greenzweig, Y. 1996, Icarus, 124, 62

Press, W. H., Teukolsky, S. A., Vetterling, T., & Flannery, B. P. 1992, Numerical Recipes in C (Cambridge: Cambridge Univ. Press)

Queloz, D., Eggenberger, A., Mayor, M., Perrier, C., Beuzit, J. L., Naef, D., Sivan, J. P., & Udry, S. 2000, A&A, 359, L13

Reiger, S. H. 1963, AJ, 68, 395

Sato, B., et al. 2005, ApJ, 633, 465

Seager, S., & Mallén-Ornelas, G. 2003, ApJ, 585, 1038

Seager, S. 2008, Space Science Reviews, 11

Southworth, J. 2008, MNRAS, 386, 1644

Sozzetti, A., Torres, G., Charbonneau, D., Latham, D. W., Holman, M. J., Winn, J. N., Laird, J. B., & O'Donovan, F. T. 2007, ApJ, 664, 1190

Szentgyorgyi, A. H., et al. 2005, Bulletin of the American Astronomical Society, 37, 1339

Tegmark, M., et al. 2004, Phys. Rev. D, 69, 103501

Thompson, A. R., Moran, J. M., & Swenson, G. W., Jr. 2001, Interferometry and synthesis in radio astronomy, 2nd ed. (New York: Wiley)

Torres, G., Winn, J. N., & Holman, M. J. 2008, ApJ, 677, 1324

van Leeuwen, F. 2007, in Hipparcos, the New Reduction of the Raw Data, Astrophysics and Space Science Library, Vol. 350 (Dordrecht: Springer)

Vogel, H. C. 1890, Astronomische Nachrichten, 123, 289

Vogt, S. S., et al. 1994, Proc. SPIE, 2198, 362

Winn, J. N., et al. 2005, ApJ, 631, 1215

Winn, J. N., Holman, M. J., & Roussanova, A. 2007, ApJ, 657, 1098

Winn, J.N. 2008, to appear in Proc. IAU Symp. No. 253, "Transiting Planets," eds. F. Pont et al. (Cambridge Univ. Press)

Winn, J. N., et al. 2008, ApJ, 683, 1076

Wright, J. T. 2005, PASP, 117, 657

Yi, S., Demarque, P., Kim, Y.-C., Lee, Y.-W., Ree, C. H., Lejeune, T., & Barnes, S. 2001, ApJS, 136, 417

Young, A. T. 1967, AJ, 72, 747

Table 2. Relative Photometry of HD 17156

Observatory Code[a]	Heliocentric Julian Date	Relative flux
1	2454459.56340	1.0041
1	2454459.56360	1.0019
1	2454459.56490	1.0017
1	2454459.56500	1.0006
1	2454459.56630	0.9954
1	2454459.56650	1.0005
1	2454459.56800	1.0016
1	2454459.56920	0.9964
1	2454459.57060	0.9974
1	2454459.57090	1.0018
1	2454459.57210	1.0009
1	2454459.57230	1.0011

[a](1) T8, T10, and T11 APT 0.8m telescopes, Fairborn Observatory, Arizona, USA. (2) Fred L. Whipple Observatory 1.2m telescope, Arizona, USA.

Note. — The time stamps represent the Heliocentric Julian Date at the time of mid-exposure. We intend for this Table to appear in entirety in the electronic version of the journal. An excerpt is shown here to illustrate its format. The data are also available from the authors upon request.

Table 3. System Parameters of HD 17156

Parameter	Value	68.3% Conf. Limits	Comment
Transit and orbital parameters:			
Orbital period, P [d]	21.21688	± 0.00044	A
Midtransit time [HJD]	2454459.69987	± 0.00045	A
Planet-to-star radius ratio, $R_p/R_\star$	0.0727	± 0.0016	A
Orbital inclination, i [deg]	86.2	-0.8, $+2.1$	A
Scaled semimajor axis, $a/R_\star$	22.8	-1.7, $+2.2$	A
Transit impact parameter, $b_{\rm I}$	0.55	-0.29, $+0.03$	A
Transit duration [hr]	3.177	-0.041, $+0.071$	A
Transit ingress or egress duration [hr]	0.25	-0.026, $+0.078$	A
Velocity semiamplitude, K [m s^{-1}]	272.7	± 2.1	A
Orbital eccentricity, e	0.6753	± 0.0036	A
Argument of pericenter, ω [deg]	121.64	± 0.48	A
Planet-to-star mass ratio, $M_p/M_\star$	0.00244	± 0.000029	C
Semimajor axis [AU]	0.1623	-0.0020, $+0.0015$	C
Stellar parameters:			
Mass, $M_\star$ [M$_\odot$]	1.263	-0.047, $+0.035$	C
Radius, $R_\star$ [R$_\odot$]	1.446	-0.067, $+0.099$	C
Surface gravity, $\log g_\star$ [cgs]	4.219	-0.055, $+0.033$	C
Mean density, $\rho_\star$ [g cm^{-3}]	0.589	-0.103, $+0.066$	A
Effective temperature, $T_{\rm eff}$ [K]	6079	± 80	B
Metallicity, [Fe/H]	$+0.24$	± 0.05	B
Projected rotation rate, $v \sin i_\star$ [km s^{-1}]	2.6	± 0.5	B
Luminosity [L$_\odot$]	2.55	-0.32, $+0.24$	C
Absolute V magnitude	3.78	-0.27,$+0.23$	C
Age [Gyr]	3.06	-0.76, $+0.64$	C
Planetary parameters:			
M_p [M$_{\rm Jup}$]	3.212	-0.082,$+0.069$	C
R_p [R$_{\rm Jup}$]	1.023	-0.055,$+0.070$	C
Surface gravity, g_p [m s^{-2}]	76.1	-9.0,$+7.3$	A
Mean density, ρ_p [g cm^{-3}]	3.72	± 0.67	C

Note. — (A) Based on the joint analysis of photometric and RV data (see § 3.1-3.3). (B) From Fischer et al. (2007), with enlarged error bars for $T_{\rm eff}$ and [Fe/H]. (C) Functions of group A and B parameters, supplemented as needed by an isochrone analysis (see § 4), the Tycho-2 apparent magnitudes (Høg et al. 2000), and *Hipparcos* parallax of $\pi = 13.34 \pm 0.72$ mas (van Leeuwen 2007).

Table 4. Fitted Limb-Darkening Coefficients for HD 17156

Bandpass	Linear Coefficient (u_1)	Quadratic Coefficient (u_2)
z	$0.13^{+0.30}_{-0.06}$	$0.00^{+0.25}_{-0.13}$
$(b+y)/2$	$0.21^{+0.42}_{-0.10}$	$0.64^{+0.13}_{-0.51}$

Table 5. Comparison of Methods for Measuring Midtransit Times

Analysis method	Midtransit time [HJD]	
	FLWO	APT
MCMC with $\beta > 1$	$2454459.70044 \pm 0.00075$	$2454459.69972 \pm 0.00065$
Random draws with replacement	$2454459.70034 \pm 0.00054$	$2454459.69974 \pm 0.00063$
Residual permutation	$2454459.70048 \pm 0.00090$	$2454459.69981 \pm 0.00095$

Table 6. Midtransit Times of HD 17156b

Heliocentric Julian Date	1σ Uncertainty	Reference
2454353.61000	0.02000	Barbieri et al. (2007)
2454438.48271	0.00067	Gillon et al. (2008)
2454374.83380	0.00200	Irwin et al. (2008)
2454417.26450	0.00210	Narita et al. (2008)
2454459.70044	0.00075	This work (FLWO)
2454459.69972	0.00065	This work (APT)

Table 7. Predicted Superior Conjunction Parameters for HD 17156b

Parameter	Value	68.3% Conf. Limits
Midpoint of superior conjunction [HJD]	2454464.627	-0.090, $+0.100$
Probability of occultation, $P(b_{\rm II} < 1 + R_p/R_\star)$	18%	$\cdots$
Probability of non-grazing occultation, $P(b_{\rm II} < 1 - R_p/R_\star)$	15%	$\cdots$
Occultation duration for an edge-on orbit [hr]	12.9	-0.9,$+1.4$
Reflected-light figure of merit, $10^6\ (R_p/d_{\rm II})^2$	4.68	-0.22, $+0.31$

Note. — The midpoint of superior conjunction has *not* been corrected for the light-travel time across the system. The result for $(R_p/d_{\rm II})^2$ is conditioned on the occurrence of occultations.